COMPARATIVE STUDY OF LES FOR TURBULENT BUOYANT FLOW IN TERMS OF SGS MODEL AND GRID RESOLUTION

Shia-Hui Peng*
Department of Thermo and Fluid Dynamics
Chalmers University of Technology
SE-412 96 Gothenburg, Sweden
peng@tfd.chalmers.se

Lars Davidson
Department of Thermo and Fluid Dynamics
Chalmers University of Technology
SE-412 96 Gothenburg Sweden
lada@tfd.chalmers.se

ABSTRACT

Subgrid scale (SGS) modelling and grid resolution in large eddy simulation (LES) are addressed for computing turbulent buoyant flow in a confined cavity with two differentially heated side walls. The SGS models compared are all based on the eddy viscosity concept but are subject to variation in formulating the buoyancy effect. It is shown that energetic flow structures enhanced by buoyancy in the boundary layer along the heated/cooled vertical wall exist in the outer layer neighboring the nearly stagnant core region of the cavity. A k^{-3} buoyancy subrange is identified in large wavenumbers to appear in both the turbulent dynamic and thermal energy spectra next to the $k^{-5/3}$ subrange.

INTRODUCTION

The buoyancy in turbulent natural convection flows interferes significantly with the evolution of turbulence and consequently affects the flow structure and transport process. Modelling the effect of buoyancy on turbulence remains a notable challenge. In large eddy simulation, the subgrid-scale stress tensor and heat flux vector nestled in the filtered governing equations represent the energy drain between the resolved large-scale eddies and the subgrid-scale eddies. Their modelling is essential to the success of a LES.

Although a variety of SGS models has been developed, models based on SGS eddy viscosity, ν_t, remain in common use. The Smagorinsky model formulates ν_t solely with the large-scale flow strain. For turbulent thermal flows, the Eidson model (Eidson 1985) includes a buoyancy-related term in the ν_t formulation. To observe how the buoyancy imposes its effect on subgrid scales via SGS viscosity, a comparative study of models as such may provide some modelling implications, particularly for flows with strong thermal stratification. Moreover, a refined grid is required in LES to resolve the near-wall, small sized, yet rather energetic flow structures. A part of this work is also devoted to an investigation of the effect of computational grid associated with the resolution of flow structures for a wall-bounded, thermal buoyant flow.

MODELLING APPROACHES

The model employed in this work includes the Smagorinsky model and the Eidson model. They can be written in a general form in terms of the reciprocal of SGS time scaling, Ω_{sgs}, viz. $\nu_t = C\Delta^2\Omega_{sgs}$, where Δ is the filter size. In the Smagorinsky model, $\Omega_{sgs} = |\bar{S}|$. The influence of buoyancy is explicitly accounted for in the Eidson model, which reads

$$\Omega_{sgs} = \left(|\bar{S}|^2 - \frac{g\beta}{Pr_t}\frac{\partial\bar{\theta}}{\partial x_j}\delta_{2j} \right)^{\frac{1}{2}}. \qquad (1)$$

To avoid non-real solutions in situations where extensive thermal stratification exists and $\frac{g\beta}{Pr_t}\frac{\partial\bar{\theta}}{\partial x_j}\delta_{2j} > |\bar{S}|^2$, this model is modified using $|\bar{S}|$ to weight the buoyancy-related term (Peng

*Present address: Computational Aerodynamics, Division of Aeronautics, Swedish Defence Agency (FOI), SE-172 90 Stockholm, Sweden. E-mail: peng@foi.se

and Davidson 1998), which yields

$$\Omega_{sgs} = |\bar{S}| - \frac{g\beta}{Pr_t|\bar{S}|}\frac{\partial\bar{\theta}}{\partial x_j}\delta_{2j}. \quad (2)$$

The SGS thermal diffusivity is computed by $\alpha_t = C_t\nu_t/C = \nu_t/Pr_t$. For base models with constant coefficients, we set $C = 0.0441$ and $Pr_t = 0.4$ in the computation, as suggested by Eidson (1985). In addition, a damping function, $f_\mu = [1 - \exp(-y^+/25)]^2$, is used. In computations with the dynamic model, the same constant is used for the SGS Prantdl number, i.e. $Pr_t = 0.4$, albeit that C and C_t are dynamically determined.

The differential governing equations are discretized using the finite volume method with the second-order central differencing scheme in space and the Crank-Nicolson scheme for the temporal discretization. The equation system is solved using an implicit, fractional-step, time-advancement method. The buoyant flow was measured in a confined cavity with the dimensions of $L_x \times L_y \times L_z = 0.75 \times 0.75 \times 1.5$ by Tian and Karayiannis (2000). The temperature difference between the vertical hot wall (θ_{hw}, at $x = 0$) and cold wall (θ_{cw}, at $x = L_x$) is $\Delta T = 40K$, giving $Ra = 1.58 \times 10^9$. The top and bottom walls are conducting boundaries, for which measured temperature distributions are available. The measurement confirmed that the mean flow in the spanwise (z-direction) midsection was not affected by the end walls and is essentially two-dimensional. In the computation, the periodic boundary condition is assumed and a uniform grid is employed in this direction. Four cases with different arrangements of the computational domain and mesh are investigated, as specified in Table 1. In all cases, the same mesh (with 96 cells) is used in the vertical direction with a stretching grid near the horizontal walls, and 96 cells are employed in the x-direction.

Case	L_z	z-mesh	x_1^+	Δx^+_{max}	Δy^+_{max}	Δz^+
A	0.75	32	0.18	73	42	64
B	0.75	64	0.18	73	42	32
C	0.75	64	0.72	78	42	32
D	0.5	64	0.72	78	42	21

Table 1: Specification of the computational domain and spacing resolution. Note: The mesh in the x direction is clustered only near the wall in Cases A and B, but is readjusted in Cases C and D to refine the mesh in the outer region of the boundary layer as well; The mesh spacing is normalized using the friction velocity at $y = L_y/2$.

RESULTS AND DISCUSSION

In the model comparison, the computation was based on Case C and the dynamic model refers to the dynamic Smagorinsky model. It is noted here that, where applied, $\langle\ \rangle$ is used to denote the averaged quantities over time and the homogeneous spanwise space. Figures 1 and 2 show a comparison for some resolved mean flow quantities and turbulence statistics in the boundary layer near the cold wall, where the buoyant velocity, $U_0 = \sqrt{g\beta\Delta T L_y}$, has been used for normalization. Different SGS models trigger no significant variation in the mean resolved velocity and temperature, although the dynamic model gives slightly better predictions in the outer part of the boundary layer as compared with the measured data.

For the resolved turbulence statistics, the base models with constant coefficients reproduce very similar distributions in a large near-wall part of the boundary layer, while the resolved turbulence in the outer part and the core region of the cavity is apparently overestimated by the modified base model (Fig. 2). Although not shown here, it is noted that this model also overpredicts other resolved turbulence quantities (except $\langle u'v'\rangle$ and $\langle v'\theta'\rangle$). In regions near the horizontal walls, the Smagorinsky model and the Eidson model, by contrast, underestimate these quantities.

In the core region of the cavity, the recirculating fluid motion is rather weak for this relatively low Rayleigh number (Peng and Davidson 2000), whereas the vertical thermal gradient is generally positive. This suggests that the buoyancy-related term, $\frac{g\beta}{Pr_t}\frac{\partial\bar{\theta}}{\partial y}$, is larger than the strain term, $|\bar{S}|^2$, in the core region. By contrast, the strain term is the dominant one in the near-wall boundary layer.

Figure 3 (a) shows a comparison of $\langle\Omega_{sgs}\rangle$. The SGS viscosity is also shown in Figure 3 (b). Near the wall, where the influence of flow strain is much greater than that of buoyancy, the three base models reproduce similar distributions for $\langle\Omega_{sgs}\rangle$ and $\langle\nu_t\rangle$. Note that the dip in the $\langle\nu_t\rangle$ distributions for Case C is caused by the grid stretching done in the outer part of the boundary layer, by which the filter size, Δ, and consequently ν_t are reduced. Neighboring the core region and in it ($x/L_x < 0.93$), the modified model allows negative Ω_{sgs} (and thus negative ν_t) provided that the total viscosity retains positive values for numerical stability. With the Eidson model, such negative values have been artificially clipped to zero to avoid non-real solutions. The Smagoringsky model, on the other hand, does not include the buoyant effect in the ν_t formulation, always giving

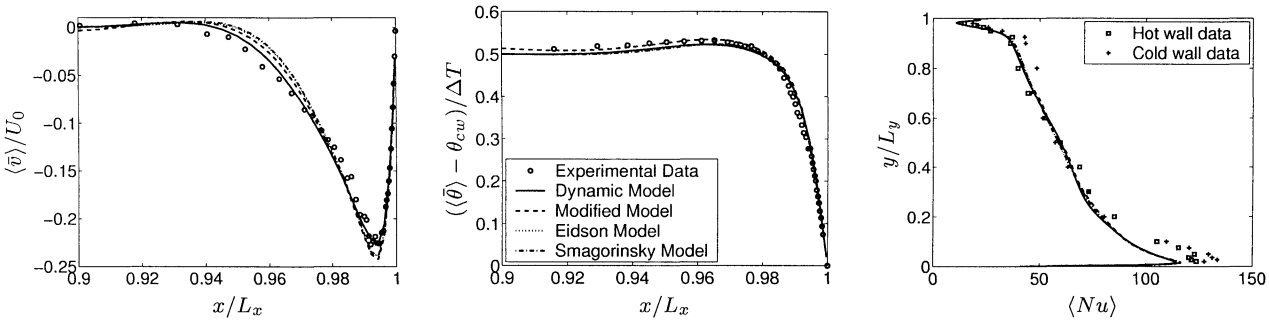

(a) Resolved vertical velocity (b) Resolved temperature (c) Nusselt number along hot wall

Figure 1: Model comparison: Resolved mean flow and thermal quantities at $y = L_y/2$ near the cold wall (with Case C).

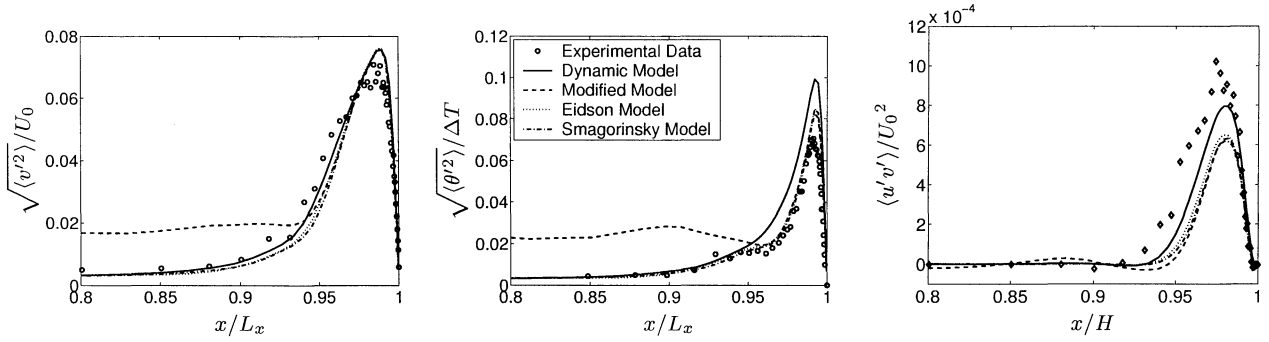

(a) Vertical velocity fluctuation (b) Temperature fluctuation (c) Turbulent shear stress

Figure 2: Model comparison: Resolved turbulence statistics at $y = L_y/2$ near the cold wall (with Case C).

$\nu_t \geq 0$. One of the intentions in the modified model is to accommodate the energy backscatter with a negative ν_t. The results in this simulation show that the weighting using $|\bar{S}|^2$ in Eq. (2) is physically inappropriate, however. The negative ν_t causes some unphysical backscatter overflow of energy in the core region. As a result, the resolved dynamic and thermal fluctuations are unreasonably amplified as shown in Figures 2 (a) and (b).

The SGS viscosity is readjusted by using the dynamic approach to the modified model, as shown in Figure 3 (c) where Cases A, B and D are computed. For comparison, the dynamic Smagorinsky model (for Case B) is also included, which produces ν_t in the outer region of the boundary layer larger than that given by the dynamic modified model. Although the dynamic modified model gives a negative coefficient, C, in a region of $x/L_x = 0.85-0.95$ (not shown here), the SGS viscosity is preserved being positive due to the negative Ω_{sgs} and thus retaining a forward energy drain.

Moreover, it is seen that the resolved turbulence level is somewhat underpredicted in the outer shearing layer (see, e.g. Fig. 2 (a)). This is partly associated with an overestimation in ν_t, which dampens too much energy in the resolved scales. Figure 3 (c) shows that the dynamic modified model yields ν_t in the outer part smaller than that given by the dynamic Smagorinsky model in Case B. Consequently, the level of resolved turbulence fluctuations may be enhanced, as desired. In the study of grid resolution, we focus hereafter on the simulation by the dynamic modified model.

Figures 4 and 5 compare the results for four different grid specifications (see Table 1). With Case B, the prediction is greatly improved over Case A by doubling the mesh in the spanwise direction. Using the same number of cells as in Case B, the results are further enhanced in Case C by clustering the mesh in the outer region of the boundary layer. Among the four cases, Case D yields the best prediction, in which the computational domain size is reduced by one-third in the spanwise direction and, consequently, the spanwise grid spacing is further refined with $\Delta z^+ \approx 21$ as compared to $\Delta z^+ \approx 32$ used in Case C. The thermal field (Figures 4 (b) and 5 (b)) is relatively less sensitive to the grid resolution but the resolved thermal flunctuation is appreciably overpredicted in all cases. This overprediction may be largely attributed to the use of a constant Pr_t. For this flow, $Pr_t = 0.4$ used in Eqs (1) or (2) is too small to sufficiently dampen the resolved thermal fluctuation. Indeed, a dynamic deter-

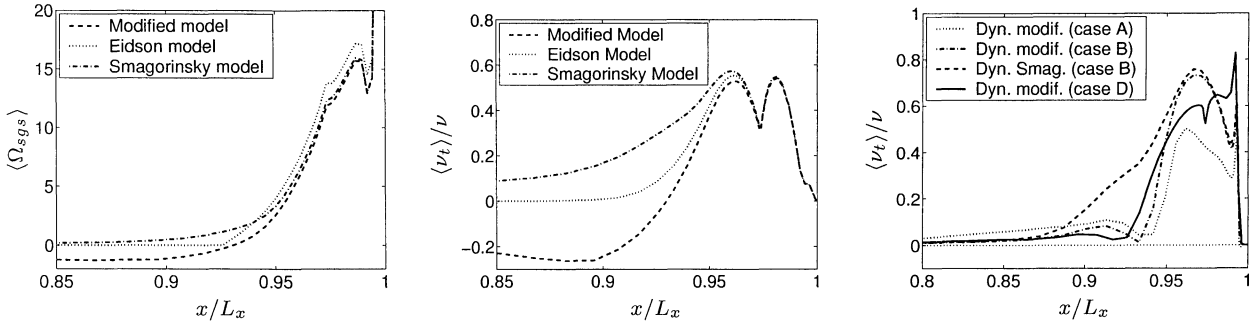

(a) SGS time scaling (b) SGS eddy viscosity (c) SGS viscosity (dynamic models)

Figure 3: Comparison of time-averaged SGS quantities at $y = L_y/2$ near the cold wall. Note that (a) and (b) are plotted for models with constant coefficients from Case C, and the results in (c) are computed with dynamic models.

mination of Pr_t as done in Peng and Davidson (1998) should be applied.

In LES the size of the smallest resolved structures is set by the grid resolution. In previous work (Peng and Davidson 2000), energetic structures were identified close to the wall in the boundary layer. Figure 6 shows that such structures actually penetrate over the whole inner part and extend further to the outer shearing layer next to the core region of the cavity (Fig. 6 (c)). The longitudinal structures, contoured with instantaneous vertical velocity fluctuations, v', become elongated up to the top horizontal wall. They emerge alternatingly in the spanwise direction with much smaller extension, and generally $\Delta z^+ \approx 65 - 105$.

Figure 7 plots the contours for instantaneous fluctuations near the hot wall in an xz-plane ($y/L_y \approx 0.6$). As is seen, the high-speed structures penetrate nearly over the whole boundary layer. In contrast to the behavior of near-wall streaky structures observed in forced convection boundary layers, the accelerating fluid elements in the vertical direction ($v' > 0$ in Figure 7 (a)) in this flow correspond in general to fluid moving away from the wall ($u' > 0$ in Figure 7 (b)). Unlike the forced convection boundary layer with high freestream momentum, the fluid momentum in the neighboring ambient of the buoyant boundary layer is often negligibly small. The fluid moving to the wall ($u' < 0$ near the hot wall) has very low momentum. As a result, the fluid elements in the boundary layer receiving such "sweep events" are decelerated, corresponding to the $v' < 0$ contours, as shown in Figures 7 (a) and (b). The streamwise accelerating fluid is actually associated with the "ejection event" characterized by fluid streams moving away from the wall, where $\frac{\partial \bar{v}}{\partial x} < 0$ in the outer shearing region of the boundary layer. Figure 7 (c) furthermore shows that the region with positive thermal fluctuations corresponds to the positive v' contours. This suggests that the buoyancy significantly interacts with the high-speed vertical fluid streams.

Figure 8 (a) illustrates the spanwise two-point correlation functions for the fluctuations of vertical velocity and temperature at location $(x/L_x, y/L_y, z/L_z) \approx (0.028, 0.5, 0.492)$. The rapid decay of both R_{vv} and $R_{\theta\theta}$ indicates that the spanwise extent of turbulence structures are rather small, as shown in Figure 6 (b) at the same location. Figures 8 (b) and (c) present the one-dimensional energy spectra for v' and θ', both of which exhibit a k_z^{-3} buoyancy subrange in large wavenumbers next to the $k_z^{-5/3}$ inertial subrange. This is consistent with Lumley's assertion for stably stratified fluid (Lumley 1964).

CONCLUSIONS

The base models studied with constant coefficients show similar performance in a large near-wall part of the boundary layer, where the effect of flow strain dominates over the influence of buoyancy. For the outer shearing layer and in the core region of the cavity, where the buoyancy effect overwhelms the flow strain, the Smagorinsky model is probably more appropriate although it does not explicitly account for the buoyancy effect in the ν_t formulation. Where the buoyancy effect is significant and with a large, positive thermal gradient, the Eidson model artificially *eliminates* SGS turbulence for numerical manipulation, whereas the choice of $|\bar{S}|$ as the weighting factor in the modified model does not either seem appropriate as it introduces excess backscatter energy into the resolved turbulence. Its dynamic variant, however, is able to readjust the SGS viscosity and reproduce reasonable results. In this case, it is

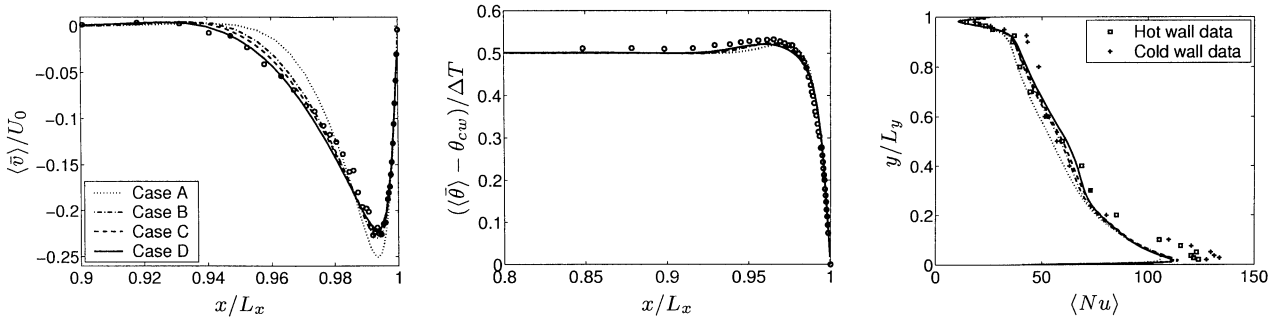

(a) Resolved vertical velocity (b) Resolved temperature (c) Nusselt number along hot wall

Figure 4: Effect of grid resolution: Resolved mean quantities with the dynamic modified model at $y = L_y/2$ near the cold wall.

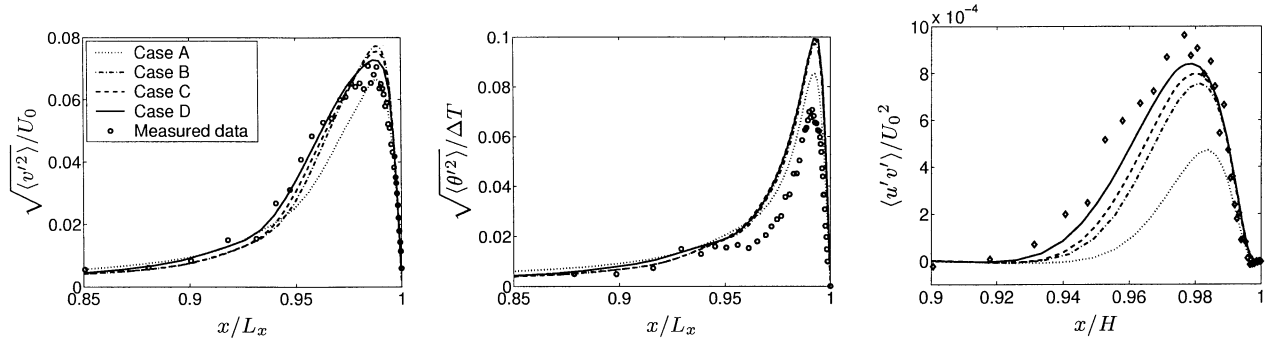

(a) Vertical velocity fluctuation (b) Temperature fluctuation (c) Temperature fluctuation

Figure 5: Effect of grid resolution: Resolved turbulent statistics with dynamic modified model at $y = L_y/2$ near the cold wall.

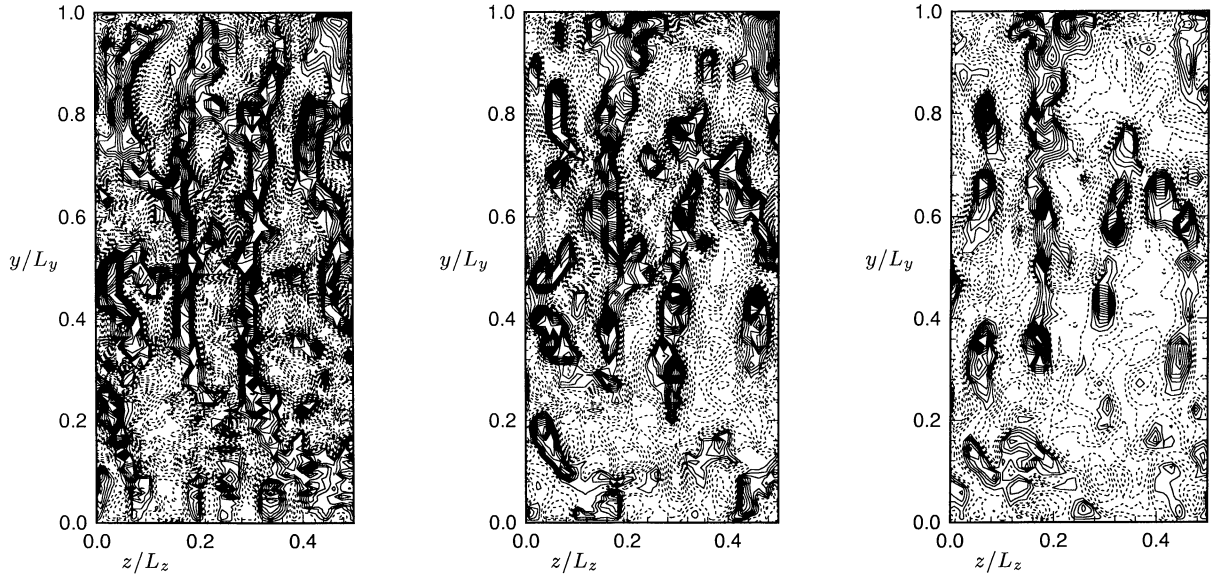

(a) At $x/L_x \approx 0.011$ ($x^+ \approx 22$) (b) At $x/L_x \approx 0.028$ ($x^+ \approx 56$) (c) At $x/L_x \approx 0.046$ ($x^+ \approx 92$)

Figure 6: Near hot-wall instantaneous v' contours at yz-planes (with Case D). Only a half of spanwise extension is taken. The contour lines are plotted with an equal interval of 0.02 in the range of $[-0.2, 0.2]$ of which positive values are represented by solid lines and negative values by dashed lines. x^+ is estimated based on the friction velocity at $y = L_y/2$.

also justified to have the Pr_t number dynamically determined.

Using a refined mesh in the outer shearing region of the boundary layer, as well as in the spanwise direction, may greatly improve the prediction. A spanwise mesh spacing of $\Delta z^+ \approx 20$ should be appropriate to resolve the energetic, coherent structures in the boundary layer, which become longitudinally elongated in the streamwise direction but have a much smaller spanwise extent. Accompanied with flow shearing, such structures exist across

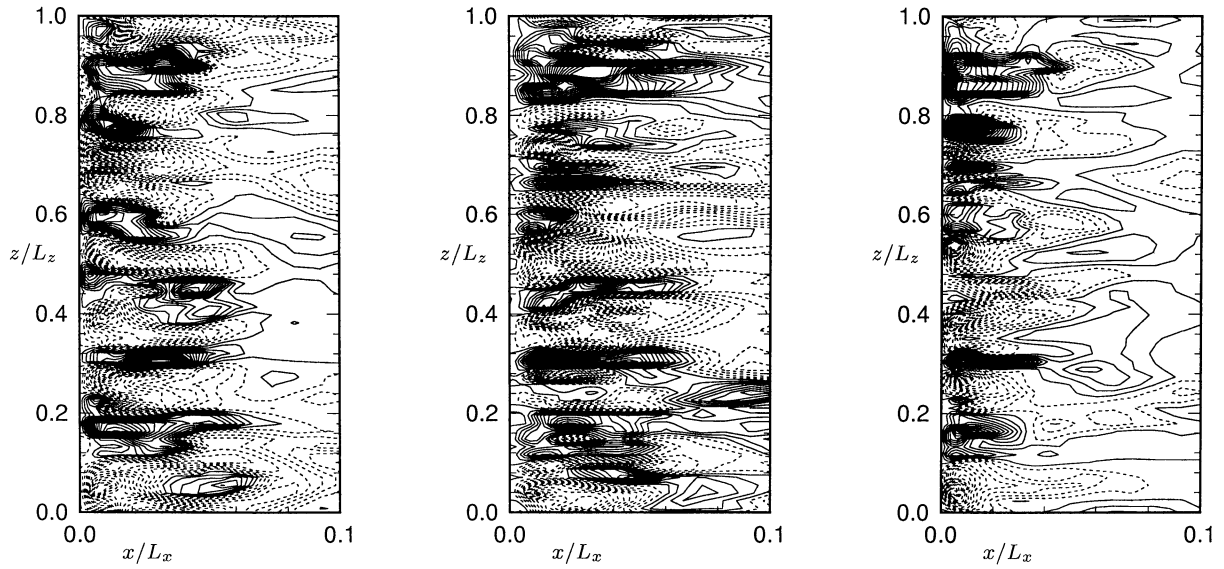

(a) Contour for v' (b) Contour for u' (c) Contour for θ'

Figure 7: Near hot-wall instantaneous contours for fluctuations at an xz-plane ($y/L_y \approx 0.6$, with Case D). The intervals for v', u' and θ' are 0.02, 0.003 and 0.5 in the ranges of $[-0.2, 0.2]$, $[-0.06, 0.06]$ and $[-10, 10]$, respectively.

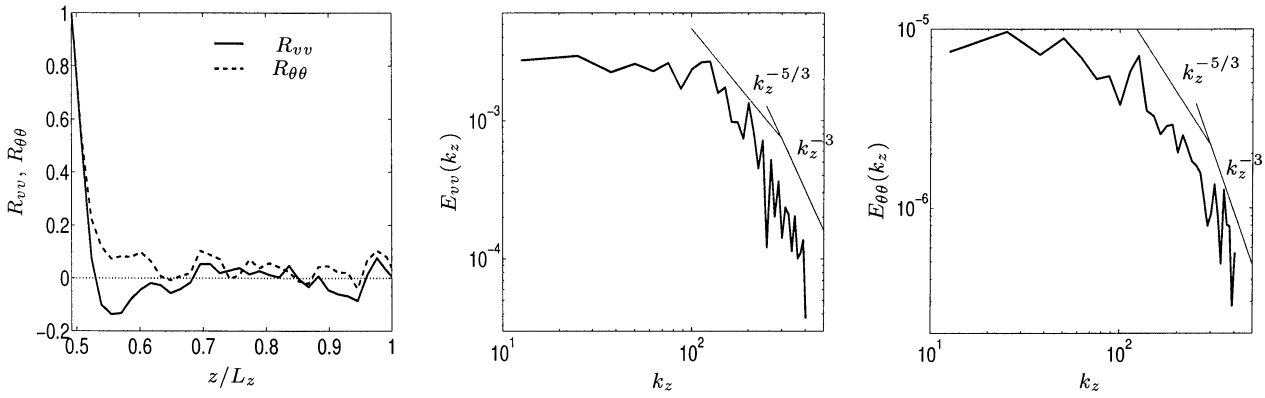

(a) Two-point correlation (b) Spectrum for vertical velocity. (c) Spectrum for temperature

Figure 8: Spanwise two-point correlation and one-dimensional energy spectra for vertical velocity and temperature (at $x/L_x \approx 0.028$, $y/L_y \approx 0.5$ and $z/L_z \approx 0.492$, with Case D).

nearly the whole boundary layer. Moreover, the simulation recovered a k^{-3} buoyancy subrange in large wavenumbers.

Aknowledgements: This work was supported by TFR. Computer time at UNICC, Chalmers, is gratefully acknowledged.

REFERENCES

Eidson, T. (1985). Numerical simulation of the turbulent Rayleigh-Bénard problem using subgrid modelling. *J. Fluid Mech. 158*, 245–268.

Lumley, J. L. (1964). The spectrum of nearly inertial turbulence in a stably stratified fluid. *J. Atmos. Sci. 21*, 99–121.

Peng, S.-H. and L. Davidson (1998). Comparison of subgrid-scale models in LES for turbulent convection flow with heat transfer. In *Turbulent Heat Transfer 2*, Manchester, UK, pp. 5.24–5.35. UMIST.

Peng, S.-H. and L. Davidson (2000). Numerical investigation of turbulent buoyant cavity flow using large eddy simulation. In *Turbulence, Heat and Mass Trasfer 3*, Nagoya, Japan, pp. 737–744. eds. Y. Nagano, K. Hanjalic and T. Tsuji, Aichi Shuppan.

Tian, Y. S. and T. G. Karayiannis (2000). Low turbulence natural convection in an air filled square cavity: Part I: The thermal and fluid flow field. *Int. J. Heat Mass Transfer 43*, 849–866.